Article

Sea-level rise effects on changing hazard exposure to far-field tsunamis in a volcanic Pacific Island

Rebecca Welsh [1*], Shaun Williams [1], Cyprien Bosserelle [1], Ryan Paulik [1], Josephina Chan Ting [2], Alec Wild [1], Lameko Talia [3]

[1] NIWA Taihoro Nukurangi, Te-Whanganui-a-Tara Wellington, Aotearoa New Zealand.
[2] Disaster Management Office, Ministry of Natural Resources and Environment, Apia, Samoa.
[3] Geosciences, Meteorology Division, Ministry of Natural Resources and Environment, Apia, Samoa.
* Correspondence: Rebecca.Welsh@niwa.co.nz

Abstract: Coastal flooding exacerbated by climate change is recognised as a major global threat which is expected to impact more than a quarter of people currently residing in Pacific Islands countries. While most research in the last decade has focused on understanding the dynamics and impacts of future coastal flooding from extreme sea levels, relative sea level rise (RSLR) effects on tsunami hazards are not well understood. Far-field or distant-sourced tsunamis tend to have relatively lower impacts in Pacific Island states compared with locally sourced events, but there is limited understanding on how the impact of far-field tsunamis changes over time due to RSLR. Using the hydrodynamics software BG-Flood, we modelled the Tōhoku tsunami from propagation to inundation in Samoa under incremental SLR to examine the effects that RSLR has on changing the exposure of the built environment (e.g., buildings) to a far-field tsunami. Outputs of maximum tsunami inundation and flow depth intensities which incorporate incremental SLR were then combined with digital representations of buildings and depth-damage functions in the RiskScape multi-hazard risk modelling software to assess the changes in building exposure over time. Results indicate that present day buildings exposure in Samoa to a Tōhoku-oki type far-field tsunami will increase by approx. 600% with 1 m RSLR by 2080–2130, and approx. 2,350% with 2 m RSLR by 2130–2140. These findings provide a useful baseline for tsunami hazard risk assessment under changing sea level conditions in analogous island environments.

Keywords: Tsunami hazard, risk modelling, climate change, built-environment, damage impacts, Tōhoku-oki tsunami, Samoa

1. Introduction

Coastal flooding exacerbated by climate change driven sea level rise in the 21st Century (21C) is recognized as a major existential threat that will affect the livelihoods of more than 1 billion people globally [1, 2]. This includes between a quarter to more than half of all people living in Pacific Islands [3]. Indeed, projected losses in real gross domestic product (real GDP) for major cities around the world are estimated to be significant within the next 100-years [4], potentially costing the global economy US$ trillions in losses by the year 2100 under a business-as-usual climate change scenario [5–7].

While much focus within the last decade has been on understanding the dynamics and impacts of coastal flooding due to tidal, relative sea level rise (RSLR), storm surges and extreme wave processes (e.g., [8–11]), concerns about the effects of sea level rise on exacerbating tsunami inundation impacts have increased. For example, Li et al. (2018) [12] demonstrated that sea level rise will increase both the frequency and intensity of tsunami-induced flooding by a factor of 1.5 to 4.7 in the city of Macau located along the South China Sea. Similarly, Nagai et al. (2019) [13] used maximum credible tsunami simulations in Tokyo Bay for different sea level rise scenarios to show that tsunami-induced flood risk in the cities of Yokohama and Kawasaki gradually increases through-

 doi:10.20944/preprints202304.0314.v1

out 21C, with the risk to life in these cities significantly affected once sea levels reach +1.0 m higher than at present.

More recently, Dura et al. (2021) [14] conducted an earthquake and tsunami modelling analysis that combined local probabilistic RSLR projections to show the increased potential for more frequent, relatively low magnitude earthquakes (M_w 8.0) originating at the Alaska-Aleutian subduction zone, to produce distant-source tsunamis that exceed historically observed maximum nearshore tsunami heights at Los Angeles and Long Beach Ports in California. These observations are consistent with nearshore tsunami height changes due to SLR presented by Koyano et al. (2022) [15] for the east coast of Japan, who also suggested that the effects of SLR on expected tsunami heights at coast are non-linear and vary according to location.

In the Pacific Islands region, far-field or distant-sourced tsunamis which take up to several hours from initiation to coastal impact are typically considered lower risk events compared with locally sourced tsunamis (e.g., [16]). However, there is a dearth in detailed hazard risk modelling studies which demonstrate the effects that SLR will have on exacerbating tsunami inundation risk to far-field events in Pacific Island environments. Furthermore, there is a scarcity of evidence on the temporal and critical SLR height thresholds where life and livelihoods are threatened due to SLR-exacerbated far-field tsunami inundation. In the light of evidence delineating the effects of SLR on increasing tsunami inundation risk in coastal continental settings (e.g., [12–15]), there is a need to investigate these processes in the Pacific Small Island Developing States (SIDS), a region that is highly vulnerable to the impacts of multiple geo-climatic hazards.

In this paper, we investigate the impact that incremental RSLR has on far-field tsunami inundation and exposure risk in Samoa (Figure 1), a Pacific SIDS where RSLR is further exacerbated by rapid post-2009 Samoa Earthquake subsidence [17]. Using the 2011 Tōhoku-oki tsunami as a proxy for a far-field tsunami type that can impact the city of Apia in north Upolu Island, we model the event from its source through to propagation across the Pacific Ocean and inundation in Samoa under incremental SLR scenarios (up to 2 m). Results of the inundation modelling are used along with digital representations of buildings to quantify their exposure and damage to permanent tidal flooding caused by incremental SLR, as well as identify sea-level thresholds where exposure risk to far-field tsunami inundation becomes critical. The implications of our findings on far-field tsunami risk planning in analogous Pacific Island contexts are discussed.

Preprints (www.preprints.org) | NOT PEER-REVIEWED | Posted: 13 April 2023 doi:10.20944/preprints202304.0314.v1

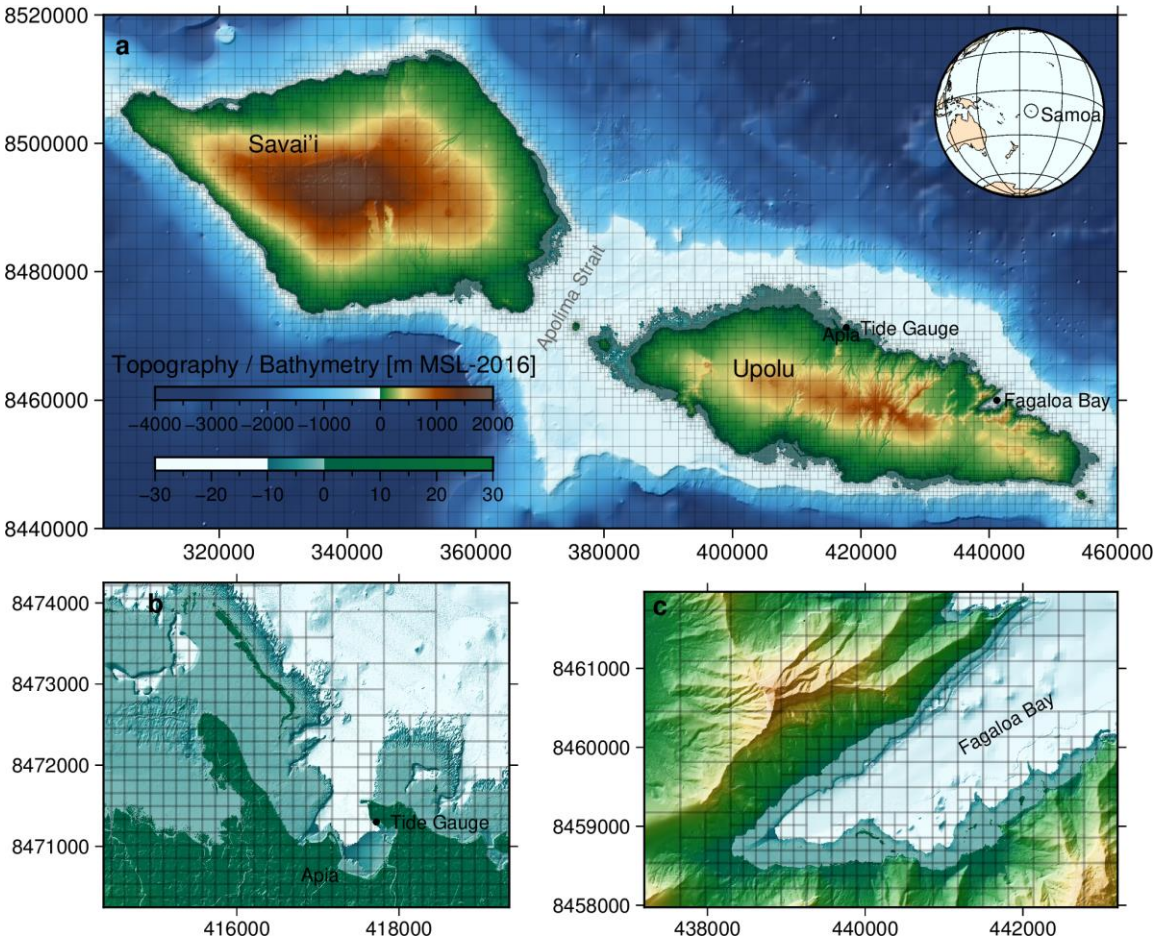

Figure 1: Samoan Islands. The inundation model bathymetry and mesh layout (transparent thin black boxes) are shown. Each black box represents a block of the adaptive mesh with each block representing 16 x 16 model cells. Apia city and Fagaloa Bay on the north of Upolu Island are directly exposed to far-field tsunamis generated from source regions along the northern Pacific Ring of Fire.

Northern coasts of the Samoan Islands are typically considered at lower threat to tsunami inundation compared with southern coasts which are exposed to the well-known tsunamigenic northern Tonga subduction zone [18]. The apparent absence of local tsunamigenic earthquake sources north of the island chain, and lack of detailed investigations on potential volcanic or landslide tsunamigenic sources off the northern flanks of the island shelf [19], leads to a general impression that tsunami threats to the capital city of Apia in north Upolu is relatively low. Indeed, historical records of tsunami impacts in Apia suggest that the threats are lower [18]. Outside of Apia, local volcanic-related tsunami threats which can impact areas in northwest Upolu (e.g., the 1907 Mt Matavanu phreatomagmatic-generated tsunamis) [20], and far-field tsunamis that can impact Fagaloa Bay in northeast Upolu have been observed (e.g., 1960 Chile tsunami) [18], although no loss of life was recorded.

A single building at the head of Fagaloa Bay is the only location in Samoa known to have experienced inundation following the 2011 Tōhoku-oki tsunami, whereby a tsunami wave of 0.7 m above normal water level was observed approx. 14 hours after the event (Figure 1). Long period waves associated with both local and distant sourced tsunamis are known to excite resonance frequencies in the characteristic V-shaped Fagaloa embayment which can amplify wave flux effects (e.g., [21]). Hence the 2011 Tōhoku-oki tsunami inundation in this embayment is unsurprising, with the observed wave providing a reference to corroborate our tsunami model and its application in the incremental SLR inundation analysis.

 doi:10.20944/preprints202304.0314.v1

2. Materials and Methods

To investigate the impact of a Tōhoku-oki type far-field tsunami inundation on the exposure of buildings in Samoa under incremental sea level rise, we: 1) modelled the tsunami from the earthquake source to inundation in the Samoan Islands as described in sections 2.1 and 2.2; and 2) modelled the built-environment exposure to tsunami inundation impacts on buildings as described in section 2.3.

2.1 Tsunami Source and Propagation Modelling

Tsunami modelling from source to propagation and inundation was undertaken using the shock-capturing hydrodynamics model BG-Flood (Block-adaptive on Graphics processing unit Flood model) [22, 23] (Figure 1). Finite faulting characteristics for the 2011 Tōhoku-oki earthquake source developed by Yamazaki et al. (2018) [24], were used to configure the tsunami generation in BG-Flood. The initial deformation of the water surface was calculated using the deformation model of Okada (1985) [25] for each of the 60 segments of the finite fault solution in [24]. The deformation of each of the 60 separate fault segments was applied at the rupture time suggested in [25] (up to 2 min after the initial rupture). Transpacific propagation of the wave to Samoa was simulated on a uniform spherical grid with a resolution of 0.05 degrees (~5 km).

BG-Flood applies Graphics Processing Units (GPU) configured with an Adaptive Mesh Refinement (AMR) type grid to simulate shallow water hydrodynamics used to model propagation across the Pacific Ocean to inundation in Samoa. The Saint-Venant, Shallow Water Equation (SWE) solver in Basilisk [26] provided the model governing equations, with a Block Uniform Quadtree mesh used to enable efficient simulation on the GPU [27]. The SWE engine validation and solver are described in detail by Popinet (2012) [28]. The ability of BG-Flood to efficiently simulate many scenarios efficiently [23], meant that it was well suited for modelling the range of 2011 Tōhoku-oki type tsunami inundation under benchmark and incremental SLR.

The digital elevation models (DEM) used in these simulations were derived from: 1) the Generic Bathymetric Chart of the Oceans (GEBCO) at ~900 m resolution covering the ocean expanse between the earthquake source and Samoa; 2) multi-beam bathymetry survey over the Samoan shelf slopes at a resolution of ~60 m [29] which was used in the adaptive refinement of the propagating wave in the nearshore; and 3) Light Detection and Ranging (LiDAR) topography and nearshore bathymetry (down to 30 m depth) at a resolution of 5 m [30], for simulation of inundation on land at spatially variable grid resolutions (e.g., 10 m on land and close to the shore and 160 m in the deep ocean).

2.2 Tsunami Inundation Modelling

Tsunami inundation modelling was undertaken in 0.2 m sea level rise increments, ranging from 0 m SLR up to 2 m SLR. These simulations were all modelled using BG-Flood with the tsunami inundating at high tide, to simulate a worse-case scenario, despite the Tōhoku tsunami reaching Samoa at low to medium tide. Additionally, the actual observed tsunami was modelled for use in validation.

The tide on 11 March 2011 was also modelled in BG-Flood under the different sea level rise increments. These results were then used in the exposure analysis to determine the assets that would already be exposed to sea level rise even without the far-field tsunami. There are no sea level records from the Apia Tide Gauge between 2 March 2011 at 0800 and 24 March 2011 at 0300 due to instrument faults, meaning that the relevant tide for the tsunami had to be predicted. This was done by first calculating the tidal constituent from the hourly tide gauge data from 1994 to 2021 using the UTide Matlab package. The constituents were then used to predict the tide level for 11 March 2011 using the tide prediction function of UTide.

The tsunami wave generated from the source and propagation modelling was added to the predicted tide from the 11 March 2011 and the SLR increment to use as the boundary forcing for the north boundary of the tsunami simulations. The tide and SLR

Preprints (www.preprints.org) | NOT PEER-REVIEWED | Posted: 13 April 2023 doi:10.20944/preprints202304.0314.v1

increment only was used as the boundary forcing for the other three sides of the tsunami simulation domain, and all domain sides for the tide simulations.

A simplified roughness map forcing was used in all simulations. The map was generated by applying a low roughness (0.0001 m) for elevations lower than –20 m (i.e., 20 m below datum) and a value of 0.01 m was used for areas with elevations above the –20 m threshold. The roughness map was used to represent the high roughness from the fringing reefs, mangroves and coastal vegetation in contrast to the relatively smooth seafloor of the continental shelf and deep ocean. Outputs of this model were in the network common data form (netCDF) file format, with the highest inundation extent extracted for use in the subsequent exposure and damage analysis.

Validation of the model was limited due to the lack of Apia Tide Gauge data. Eyewitnesses from the 2011 tsunami event in Samoa observed the inundation of only one building in Fagaloa Bay. As seen in Figure 2, the tide alone did not result in the inundation of this building, yet when coupled with the tsunami this building gets inundated as expected which helps to validate our model.

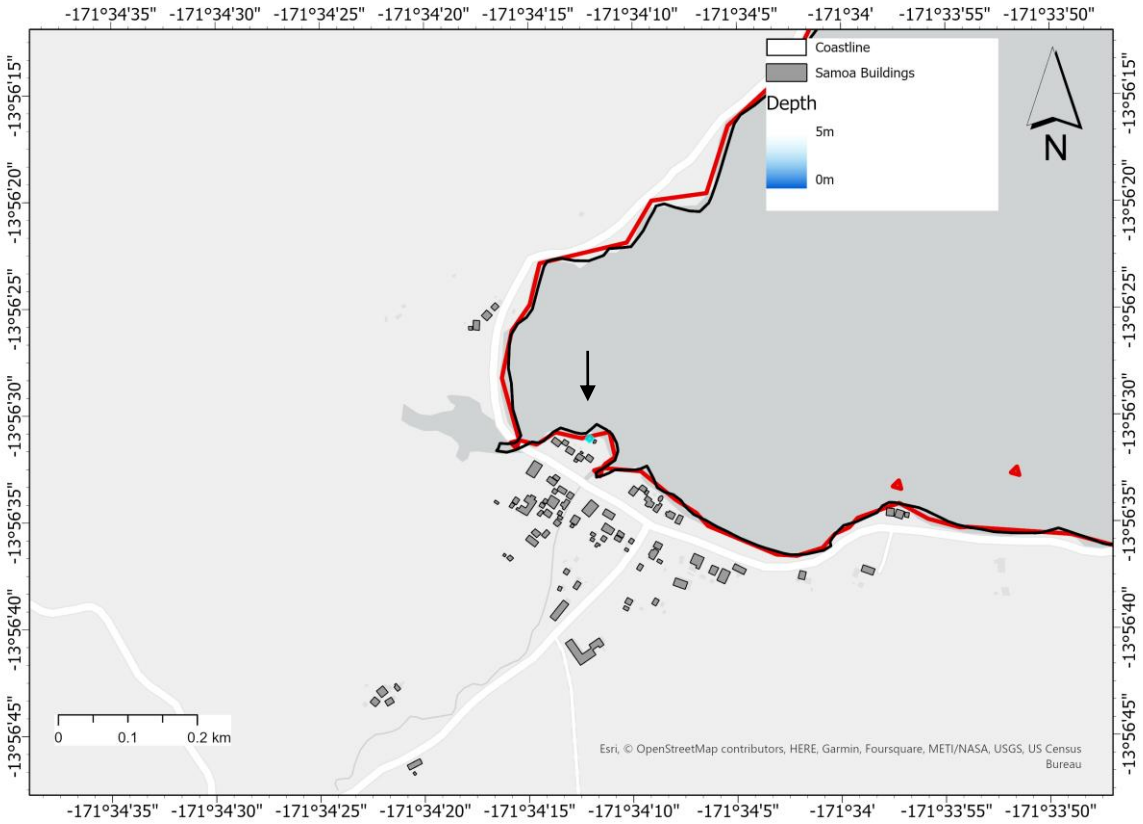

Figure 2: Maximum inundation extent of modelled tsunami wave in Fagaloa Bay. The inundated building of interest used for validation is denoted by the arrow.

2.3 Tsunami Damage Analysis

Cumulative tsunami damages in response to RSLR were analysed using the multi-hazard impact model framework supported by the RiskScape software [31]. RiskScape implements modeller-defined risk quantification workflows as model pipelines. Model pipeline steps and functions enable the analysis of hazard, exposure, and vulnerability data across different spatio-temporal domains using geoprocessing and spatial sampling operations. Pipelines configured to analyse direct physical damage to buildings in this study are presented in Figure 3, with building structures selected for damage analysis due to their socio-economic importance in tsunami preparedness, response and recovery activities.

Preprints (www.preprints.org) | NOT PEER-REVIEWED | Posted: 13 April 2023 doi:10.20944/preprints202304.0314.v1

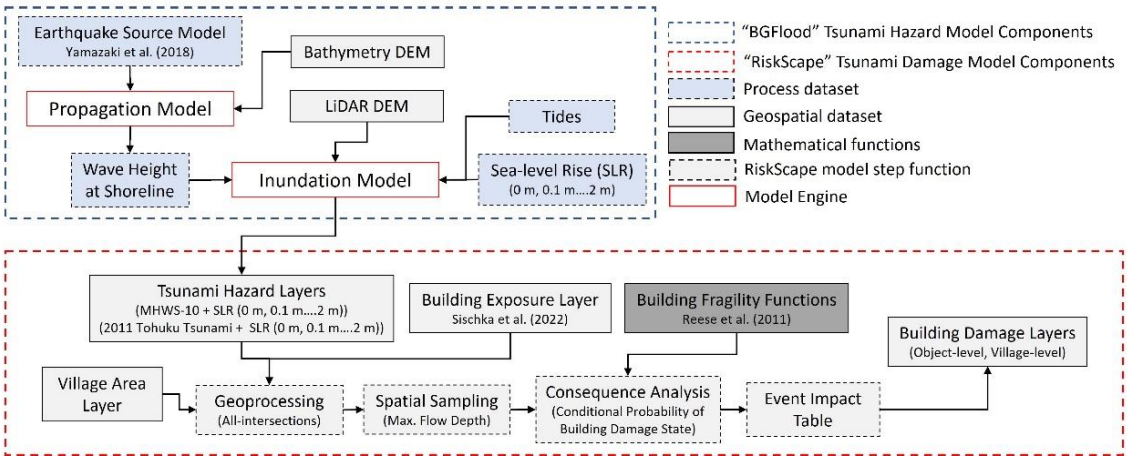

Figure 3: RiskScape framework showing the modelling workflow, data inputs and outputs.

In addition to tsunami hazard scenarios presented in Section 2.2, exposure and vulnerability information provide model inputs to quantify the direct physical damage to buildings. Buildings on located within the maximum modelled tsunami run-up extent were acquired from Sischka et al. (2022) [32]. Building outlines were represented as polygons with construction frame attribute characteristics.

To model the damages to buildings exposed to tsunami inundation, we used fragility curves which relate a tsunami hazard intensity measure (e.g., flow depth) to the conditional probability of built structures reaching or exceeding a given damage state [33]. In this study direct physical damage is estimated using empirical fragility curves that represent Samoan buildings damaged in the 2009 South Pacific Tsunami [34]. These curves denote a lognormal cumulative density function (CDF) that estimates conditional probabilities of buildings reaching specific damage states (DS) in response to maximum tsunami flow depth (m) (Table 1), and represent 'timber', 'masonry' and 'reinforced concrete' construction frame typologies. Where μ and σ coefficients are unavailable for timber and reinforced concrete typologies (Table 1), or where construction frame attributes were absent and could not be attributed to buildings, masonry fragility curves were applied to calculate the conditional DS probabilities.

Table 1: Summary of tsunami fragility curve parameters for buildings applied in this study. Masonry parameters for DS1 and DS2 were applied for timber and reinforced concrete building construction frames.

Damage State (DS)	Damage Description	Construction Frame					
		Timber		Masonry		Reinforced Concrete	
		μ	σ	μ	σ	μ	σ
0	None	-	-	-	-	-	-
DS1 Light	Non-structural damage only	-	-	0.29	0.46	-	-
DS2 Minor	Significant non-structural and minor structural damage	-	-	0.46	0.4	-	-
DS3 Moderate	Significant structural and non-structural damage	1.15	0.38	1.28	0.35	1.38	0.56
DS4 Severe	Irreparable structural damage, will require demolition	1.26	0.4	1.86	0.41	3.45	0.54
DS5 Collapse	Complete structural collapse	1.62	0.28	2.49	0.4	7.3	0.94

A model pipeline was developed to quantify the direct tsunami exposure and physical damage to buildings in RiskScape (Figure 3). Individual tsunami hazard and RSLR scenarios consisted of two digital maps representing: 1) tsunami flow depth; and 2)

Preprints (www.preprints.org) | NOT PEER-REVIEWED | Posted: 13 April 2023 doi:10.20944/preprints202304.0314.v1

permanent tide without tsunami inundation. Buildings exposed to tide inundation depths > 0.05 m were identified as permanently inundated and removed from the physical damage analysis. A maximum flow depth for built structures episodically exposed to tsunami hazards was then determined from spatial sampling of grids intersecting buildings outline polygons. Maximum flow depth was applied in object-specific building curves to calculate the conditional probability of each DS, which were then weighted to estimate the damage probability (0–1) for each building object.

3. Results

Modelling results of the 2011 Tōhoku-oki type tsunami in Samoa corroborate eyewitness observations that the impacts of inundation were minimal and predominantly confined to Fagaloa Bay in northeast Upolu. The tsunami arrival coincided with low tide and resulted in the inundation of one building located on the coastline in Fagaloa Bay (Figure 2). Under increasing SLR the impacts of a similar magnitude event are more severe. For example, Figure 4 and Figure 5 show increases in wave amplification for a Tōhoku-oki type tsunami at the coast in Apia and Fagaloa Bay with increasing sea levels, with the extent of tsunami flooding and expected damage in these locations becoming more widespread and severe.

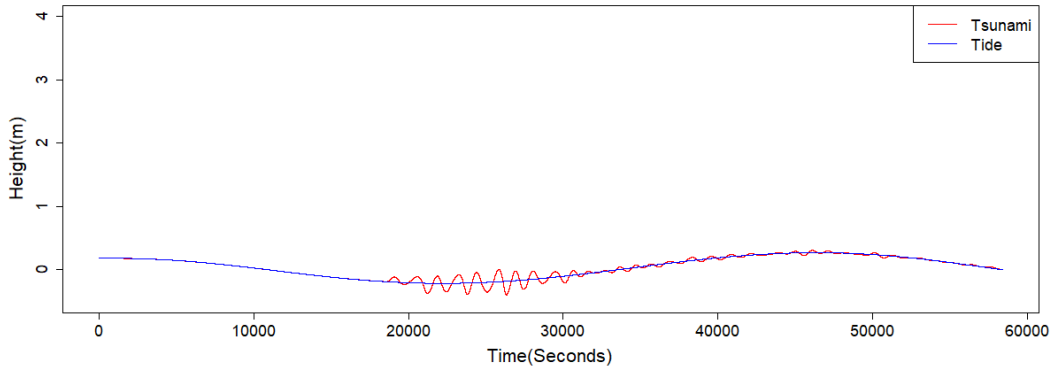

(a)

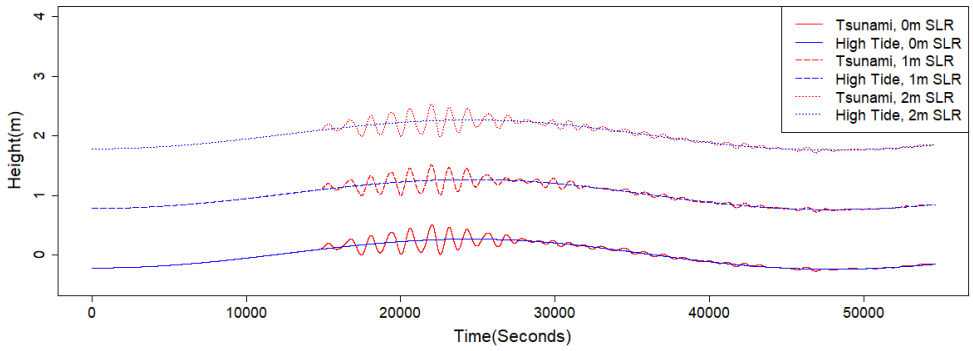

(b)

Figure 4: Time series graph showing: (a) the modelled Tōhoku tsunami wave at Fagaloa Bay; (b) the modelled Tōhoku tsunami wave arriving at high tide with 0 m SLR, 1 m SLR and 2 m SLR at Fagaloa Bay.

Preprints (www.preprints.org) | NOT PEER-REVIEWED | Posted: 13 April 2023 doi:10.20944/preprints202304.0314.v1

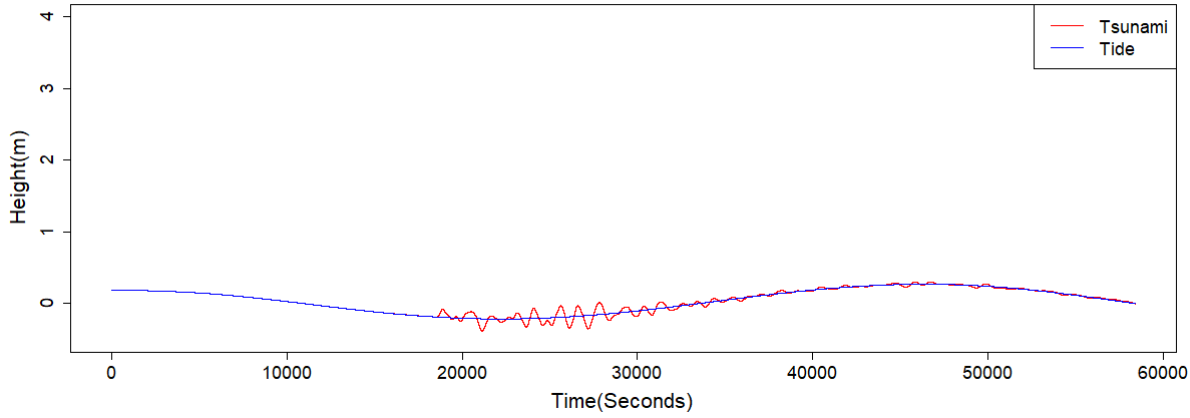

(a)

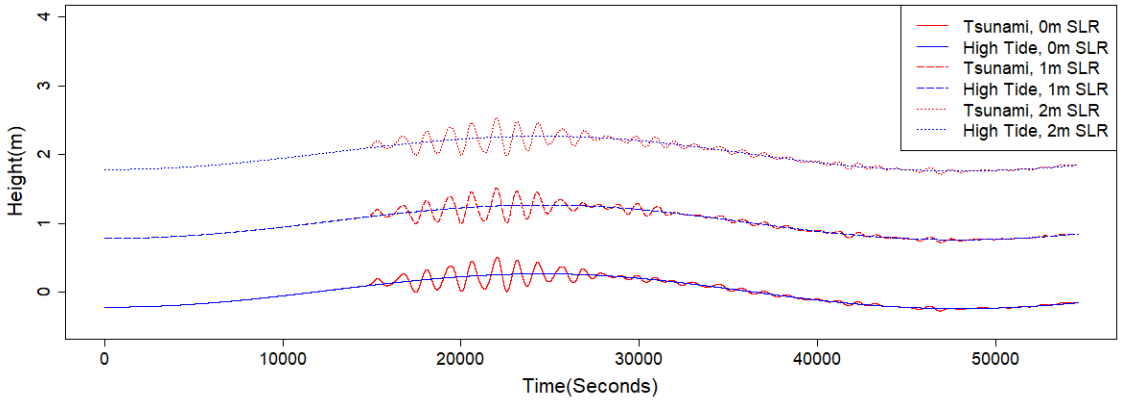

(b)

Figure 5: Time series graph showing: (a) the modelled Tōhoku Tsunami wave at the Apia Tide Gauge; (b) the modelled Tōhoku tsunami wave arriving at high tide with 0 m SLR, 1 m SLR and 2 m SLR.

Additionally, more buildings become exposed to inundation as well as experience greater severity of tsunami damaging impacts with increasing sea level rise, as evident in the higher probable damage states (Figure 6 and Figure 7). This is explained by the greater tsunami inundation extents and increases in flood depths above ground level at any given location within the inundation exposure zone under corresponding incremental SLR. This results in more buildings experiencing over a 50% probability of reaching or exceeding DS5, meaning they are likely to be completed destroyed or washed away. For example, the scenario which the tsunami arrives at high tide with 2 m of SLR destroys 1,142 buildings across the entire country compared with 250 buildings for the scenario with 1 m of SLR.

Preprints (www.preprints.org) | NOT PEER-REVIEWED | Posted: 13 April 2023 doi:10.20944/preprints202304.0314.v1

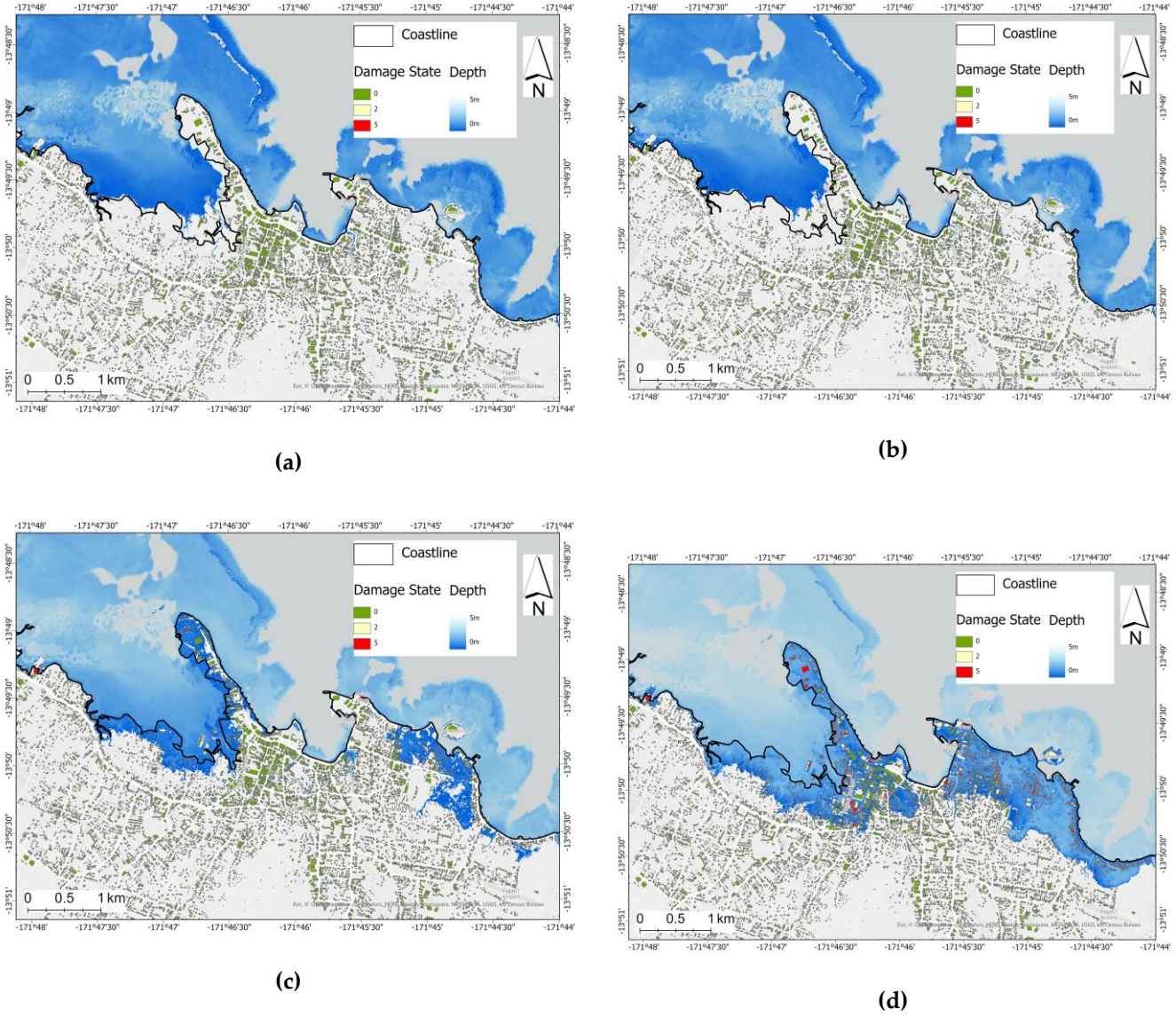

Figure 6: Most probable damage states of buildings in Apia exposed to: a) Tōhoku Tsunami wave; b) Tōhoku Tsunami wave arriving at high tide with 0 m SLR; c) Tōhoku Tsunami wave arriving at high tide with 1 m SLR; d) Tōhoku Tsunami wave arriving at high tide with 2 m SLR.

Preprints (www.preprints.org) | NOT PEER-REVIEWED | Posted: 13 April 2023 doi:10.20944/preprints202304.0314.v1

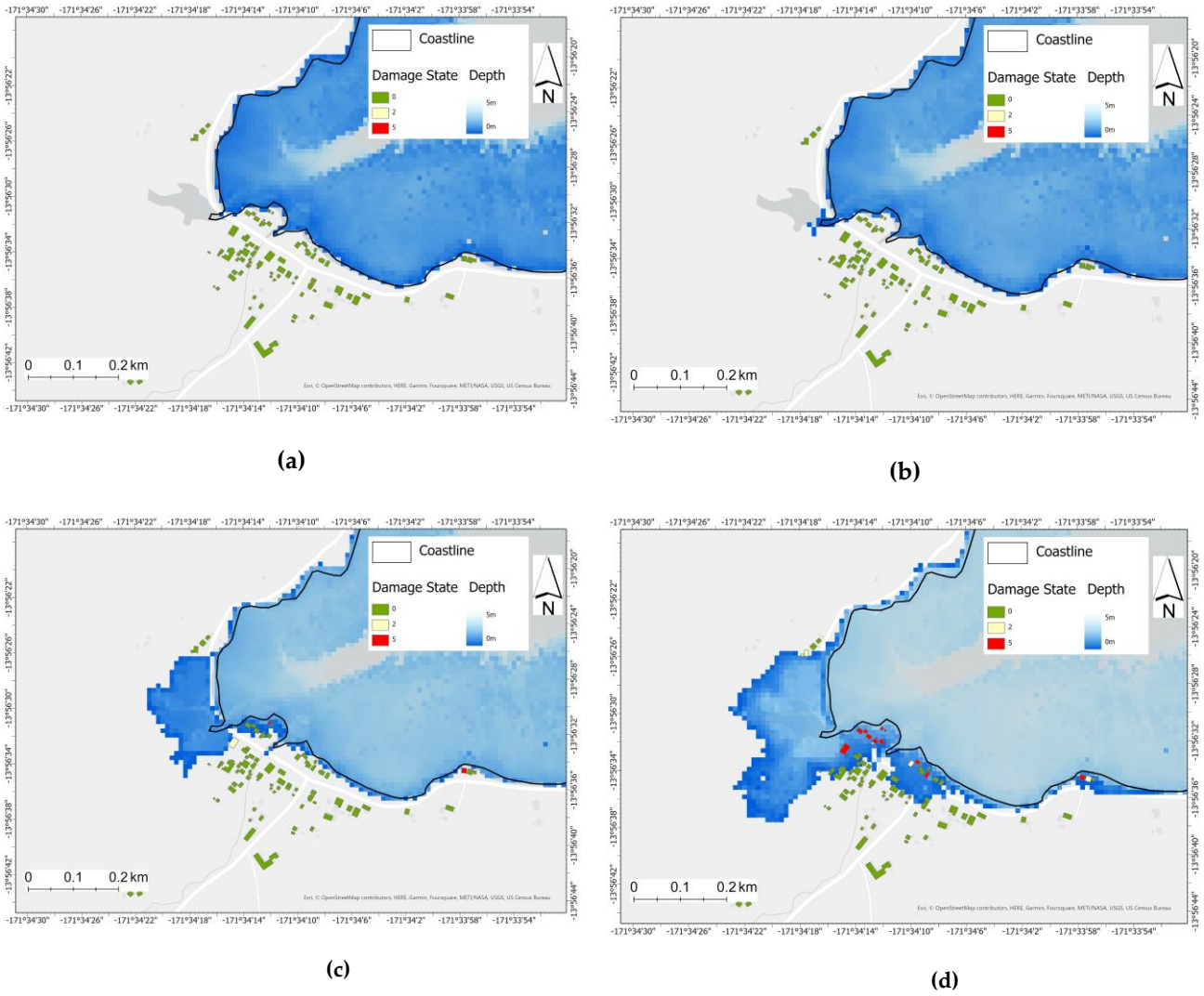

Figure 7: Most probable building damage states in Fagaloa Bay for: a) Tōhoku Tsunami wave; b) Tōhoku Tsunami wave arriving at high tide with 0 m SLR; c) Tōhoku Tsunami wave arriving at high tide with 1 m SLR; d) Tōhoku Tsunami wave arriving at high tide with 2 m SLR.

Importantly, many of the buildings inundated by this characteristic tsunami type under a 1 m SLR scenario are within the high tide inundation zone. This implies that buildings in these locations will be subjected to permanent flooding whereby habitability will likely be compromised when sea level reaches 1 m above its current level in future (e.g., Figure 8). The difference between the tsunami and permanent tide inundation extents increases dramatically after 0.6 m RSLR from 0.26 km^2 to 1.14 km^2 by 1.2 m RLSR (Figure 9a). A similar trend is observed for tsunami exposed buildings with the permanent tide inundation removed. That is, 189 buildings are exposed with 0.6 m RSLR, but 838 are exposed with 1.2 m RSLR (Figure 9b). After 1.2 m RSLR the combined tsunami and permanent tide inundation extent and number of exposed buildings becomes more even.

Preprints (www.preprints.org) | NOT PEER-REVIEWED | Posted: 13 April 2023 doi:10.20944/preprints202304.0314.v1

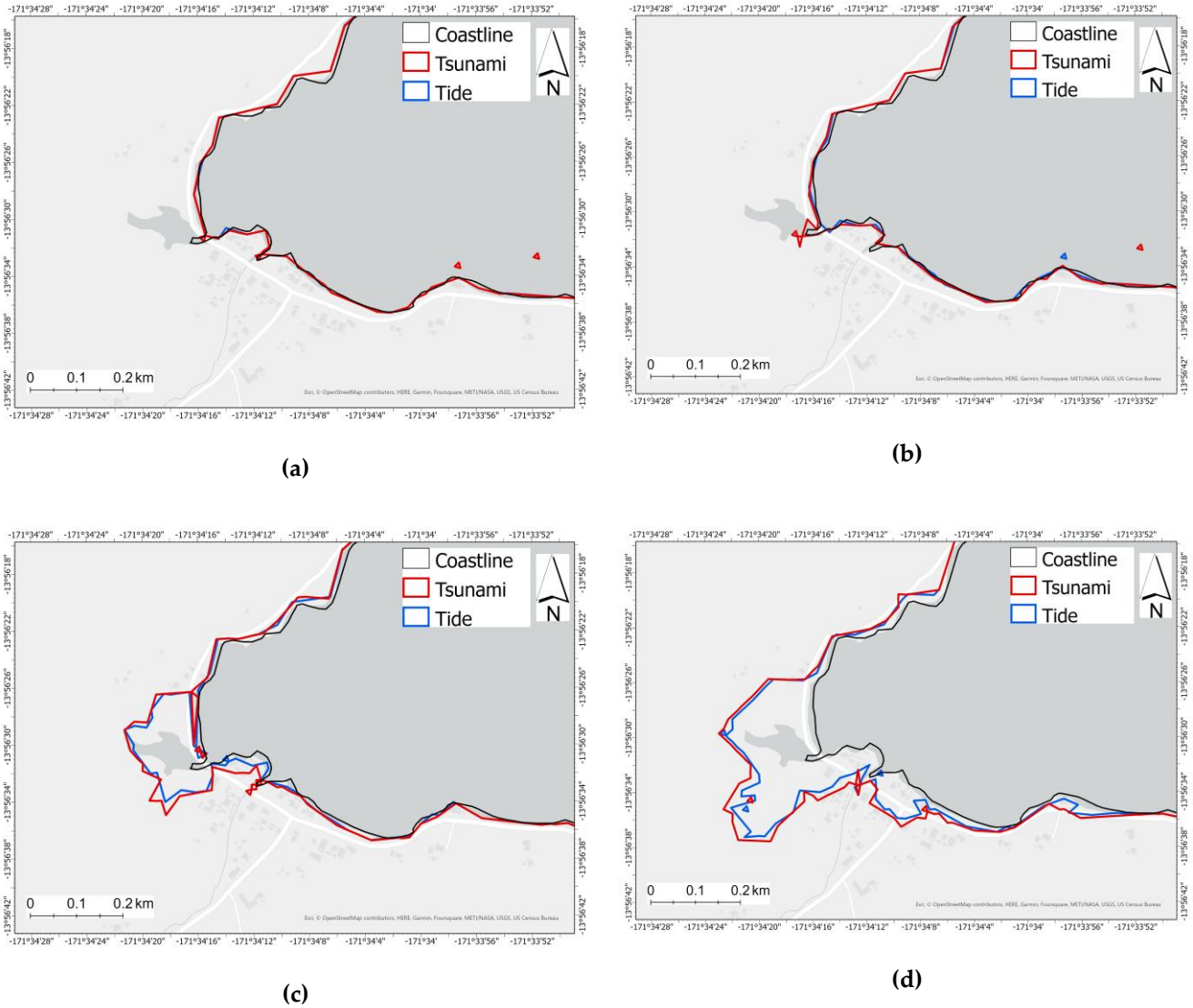

Figure 8: Tsunami and tide extents in Fagaloa Bay for: a) Tōhoku Tsunami wave and tide on 11 March 2011; b) Tōhoku Tsunami wave hitting at high tide with 0 m SLR and tide on 11 March 2011; c) Tōhoku Tsunami wave hitting at high tide with 1 m SLR and tide on 11 March 2011 with 1 m SLR; d) Tōhoku Tsunami wave hitting at high tide with 2 m SLR and tide on 11 March 2011 with 2 m SLR.

Preprints (www.preprints.org) | NOT PEER-REVIEWED | Posted: 13 April 2023 doi:10.20944/preprints202304.0314.v1

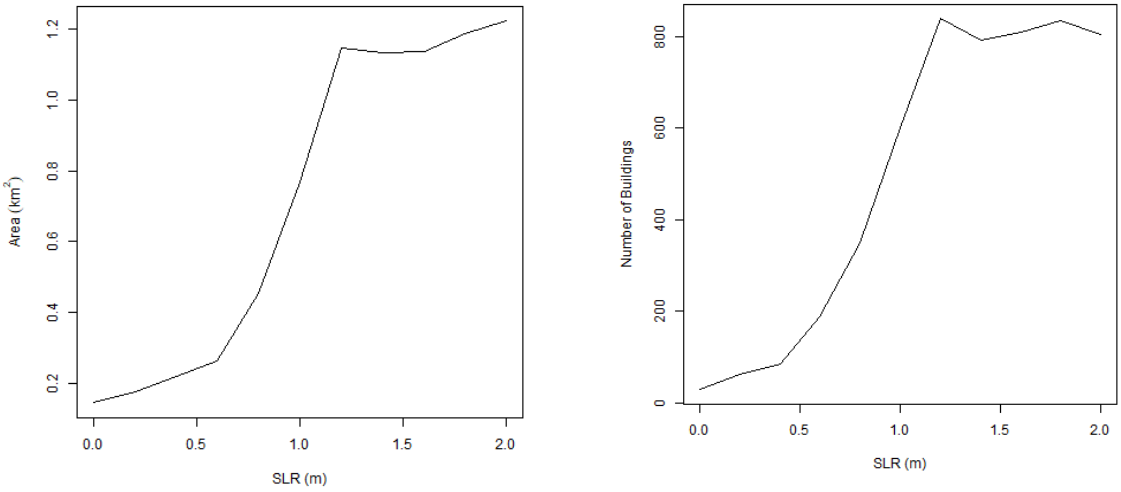

(a) **(b)**

Figure 9: Difference between tsunami and tide for: a) inundation extents; b) number of buildings exposed.

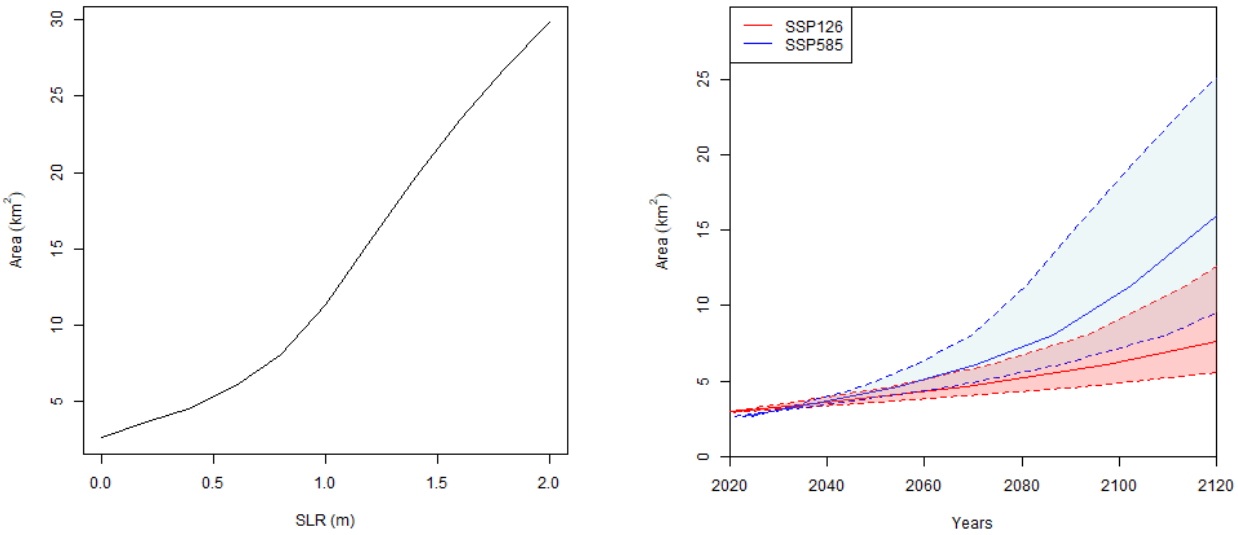

(a) **(b)**

Figure 10: Tsunami inundation extent under: a) different SLR increments; b) different SSP pathways.

These results clearly indicate that the number of buildings exposed is proportional to the inundation extent, i.e., increasing as RSLR increases (Figure 11). The maximum buildings exposed to tide is 9,056, which occurs with 2 m SLR, compared to 9,860 exposed to the tsunami, a difference of 804. Based on the Intergovernmental Panel on Climate Change (IPCC) shared socioeconomic pathway (SSP) climate change scenarios [35], by the year 2100 the likely number of buildings exposed to the tide only could be as low as 529 (SSP1–2.6, quantile 17), or as high as 4,916 (SSP5–85, quantile 83). Likewise, buildings exposed to the tsunami wave could be between 615 (SSP1–2.6, quantile 17) and

Preprints (www.preprints.org) | NOT PEER-REVIEWED | Posted: 13 April 2023 doi:10.20944/preprints202304.0314.v1

5,707 (SSP5–8.5, quantile 83). With SSP1–2.6 (quantile 17), an extra 86 buildings are exposed to the tsunami, however for SSP5–8.5 (quantile 83) an additional 791 buildings are exposed.

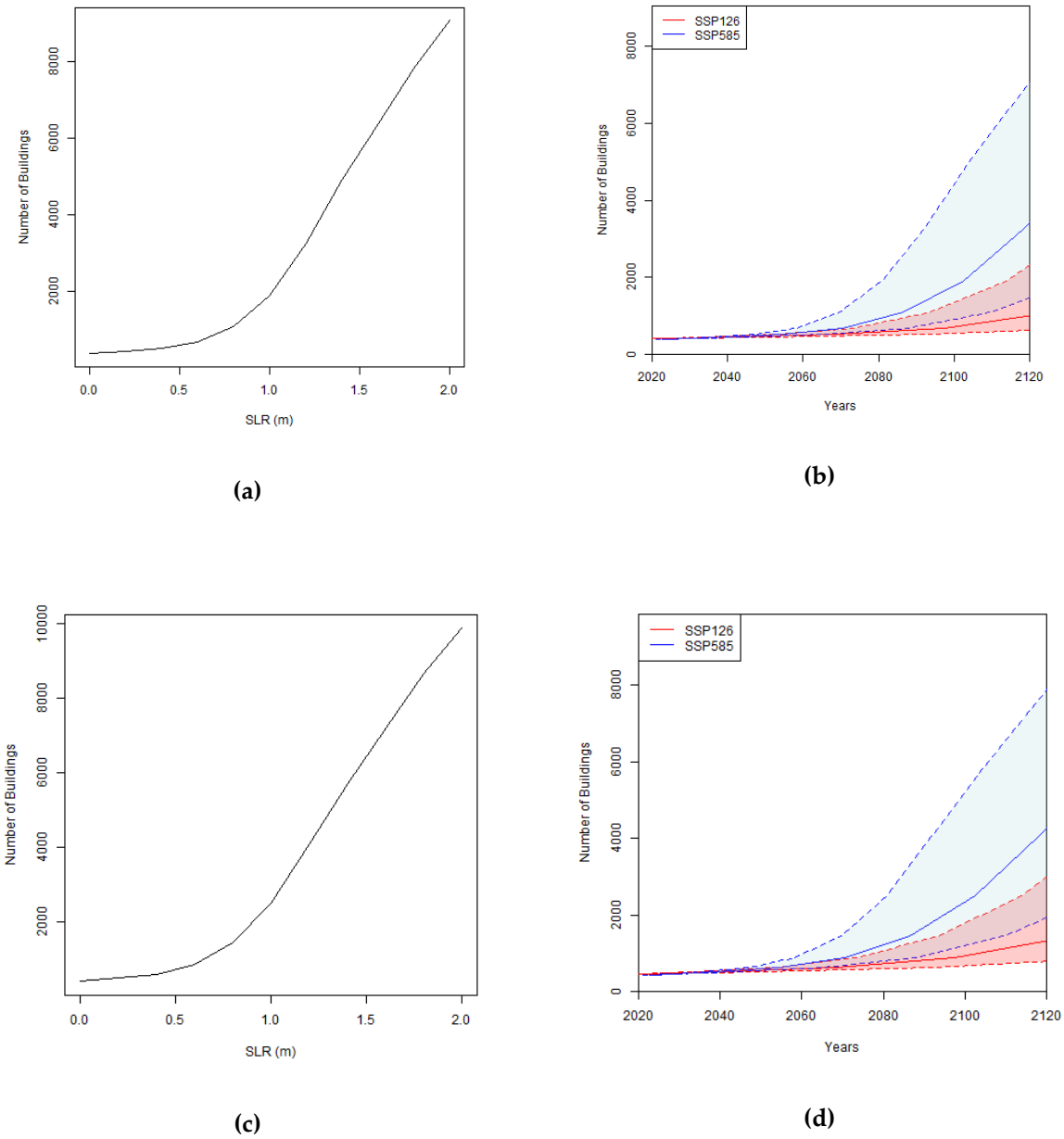

Figure 11: Buildings exposed to: a) Tide under different SLR increments; b) Tide under SSP1-26/SSP5-85; c) Tsunami under different SLR increments; d) Tsunami under SSP1-26/SSP5-85.

The number of buildings with over a 50% probability of reaching/exceeding DS5, which are likely to be fully destroyed or washed away, also increases significantly as RSLR increases (Figure 12). By 2100 it is likely that the tsunami and tide combined could result in approx. 55 buildings (SSP1–2.6, quantile 17) to 430 buildings (SSP5–8.5, quantile 83) reaching/exceeding DS5.

Preprints (www.preprints.org) | NOT PEER-REVIEWED | Posted: 13 April 2023 doi:10.20944/preprints202304.0314.v1

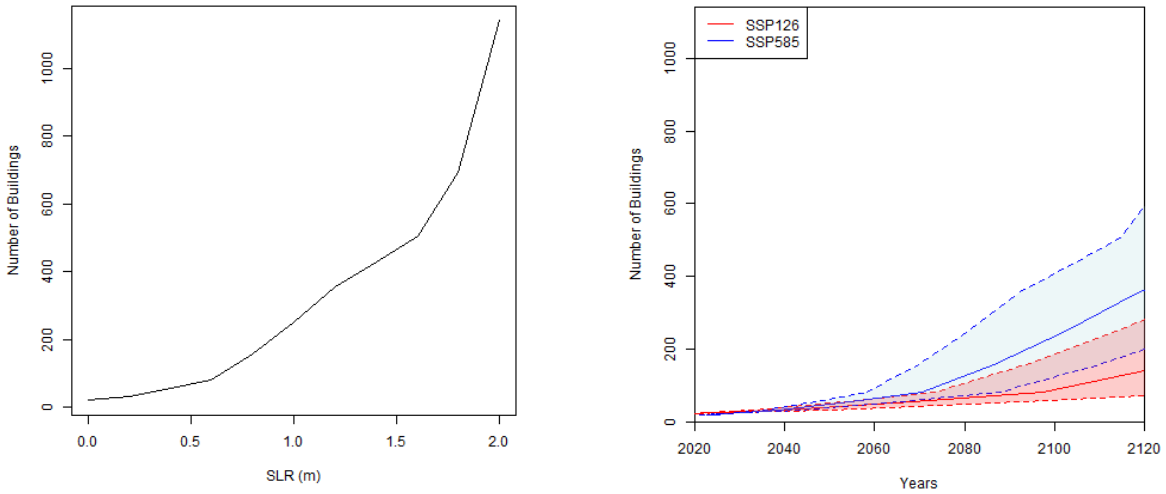

(a) **(b)**

Figure 12: Number of buildings with a 50% probability of reaching or exceeding DS5 for: a) SLR increments; b) years in response to SLR under SSP1–2.6 and SSP5–8.5.

4. Discussion

The 2011 Tōhoku-oki event represents one of the most destructive tsunamis to have occurred in the 21st century in terms of losses and damage, with far-field effects experienced in Fagaloa Bay, Samoa, approximately 7,500 km southeast of the source. Whilst the impacts of tsunami inundation from this event in Samoa were minimal, the results of our study suggest that a similar far-field type event occurring under future SLR of 1 m and 2 m can impact up to 2,082 and 9,440 more buildings, respectively, compared with present-day exposure levels. When removing the buildings already exposed to permanent tide inundation, if a similar event were to occur with 1 m and 2 m of SLR it is likely to expose 570 and 774 more buildings, respectively. These increases in exposure are explained by the greater tsunami inundation extents and corresponding flow depths above ground level under the incremental SLR scenarios assessed.

Based on sea level rise projections for Samoa under a high emission, low mitigation, shared socioeconomic pathway scenario (SSP5–8.5) with medium confidence at the 17th–83rd quantile, 0.5 m SLR is likely reached/exceeded in Samoa between the decades 2050–2080, 1 m SLR likely reached/exceeded by 2080–2130, and 2 m SLR likely reached/exceeded as early as 2130–2140 [35]. Furthermore, post-2009 South Pacific earthquake subsidence in Samoa is occurring at a particularly fast rate of 8–16 mm/year [17], which exacerbates SLR and implies that SLR of 1 m could be reached/exceeded earlier than current projections for these islands.

Interestingly, our results indicate that one of the greatest risks to buildings was the SLR itself rather than the characteristic far-field tsunami-type which we had assessed. While the modelled inundation extents combining permanent tide and tsunami consistently showed the tsunami extent being greater than the tide, the increase in sea level is what drives the extension of inundation further inland and subsequent increase in building exposure and damage. After approximately 0.6 m SLR the tsunami and permanent tide extents start to diverge more significantly, with this divergence highest after 1 m (Figure 11). This indicates that an approx. 1 m SLR threshold is where far-field tsunamis such as the 2011 Tōhoku-oki type event may become more problematic. These observations are consistent with similar findings by Nagai et al. (2020) [13], who showed that tsunami risk to life in the cities of Yokohama and Kawasaki in Japan significantly become affected once sea levels reach +1.0 m higher than at present.

While our results show compelling evidence for the effects of SLR on exacerbating far-field tsunami inundation risk throughout the 21st Century in Samoa, one of the main problems with the modelling approach taken was the absence of Apia tide gauge data for validation of the event at the time of its occurrence in 2011. This was due to the Apia tide gauge being temporarily non-operational when the 2011 event occurred. Nevertheless, eyewitness accounts of inundation collected by the Samoa Disaster Management Office in Fagaloa Bay after the event provided a means to corroborate, in part, the modelled runup in this study. Consistent modelled-to-observed results of the 2011 event in Fagaloa Bay were observed which substantiates its usage as a characteristic-type far-field event in our incremental SLR scenario modelling.

Overall, our results indicate that far-field tsunami inundation in Samoa similar to a 2011 Tōhoku-oki type event will be exacerbated throughout the 21st Century with rising sea level, posing significant coastal resilience challenges once sea levels reach/exceed +1.0 m. In contrast to high volcanic islands of the Pacific such as Samoa, our findings have major implications for tsunami inundation risk in low-lying atolls which typically have summits of less than 5–10 m above sea level. These observations lead us to suggest that incorporating the effects of SLR in tsunami hazard risk modelling assessments in Pacific Island environments should be considered for use in longer-term coastal resilience and adaptation planning.

5. Conclusions

This study set out to assess the effects that rising sea level may have on far-field tsunami inundation exposure and impacts to buildings in a Pacific Island context. Using a characteristic 2011 Tōhoku-oki type far-field tsunami scenario in Samoa, we show that incremental SLR over the 21st Century results in greater tsunami inundation extent and corresponding flood depths above ground level. In turn, this exposes more buildings to more severe damage with each progressive rise in SLR, with tsunami impacts becoming significant once SLR reaches/exceeds +1.0 m. Based on a high emissions, low-mitigation SSP5–8.5 SLR scenario for Samoa, it is likely this threshold will be reached by the decades 2080–2130 or sooner depending on whether the current rates of rapid land subsidence in Samoa continue. Overall, our findings have planning implications for similar environmental settings in the Pacific and point towards a need to incorporate the effects of SLR in future tsunami inundation risk assessments.

Supplementary Materials: Not applicable.

Author Contributions: Conceptualization, R.W., S.W., R.P. and C.B.; methodology, S.W., R.P., R.W. and C.B.; software, C.B. and R.P.; validation, C.B. and R.W.; formal analysis, R.W., S.W., C.B., R.P., J.C-T., A.W. and L.T.; investigation, R.W., C.B. and A.W.; resources, S.W and R.P.; data curation, R.P., R.W., J.C-T., L.T. and C.B.; writing—original draft preparation, R.W., S.W., R.P. and C.B; writing—review and editing, R.W., S.W., C.B., R.P., J.C-T., A.W. and L.T.; visualization, R.W. and C.B.; supervision, S.W., C.B. and R.P.; project administration, S.W.; funding acquisition, R.P. All authors have read and agreed to the published version of the manuscript.

Funding: The APC was funded by NIWA Taihoro Nukurangi Strategic Science Investment Fund Project No: CARH2305.

Institutional Review Board Statement: Not applicable.

Informed Consent Statement: Not applicable.

Data Availability Statement: The open-source BG-Flood model is available at (https://github.com/CyprienBosserelle/BG_Flood), and the code version used in this research is archived at (http://doi.org/10.5281/zenodo.3905416). The RiskScape modelling software is available at (https://riskscape.org.nz/). LiDAR data were obtained via formal request from the Samoa Ministry of Natural Resources Environment (MNRE). Results of exposed buildings produced in this study are archived at MNRE, NIWA and the Pacific Community (SPC).

Acknowledgments: This research was supported by the New Zealand National Institute of Water and Atmospheric Research (NIWA) Taihoro Nukurangi Strategic Science Investment Fund Project

No. CARH2305 (R. Welsh, S. Williams, C. Bosserelle, R. Paulik, A. Wild). J.C. Ting and L. Talia were supported through the MNRE–NIWA Collaborative Research Platform No. FY2122. The authors thank the anonymous reviewers for feedback which helped to improve the paper.

Conflicts of Interest: The authors declare no conflict of interest.

References

1. Kulp, S.A.; Strauss, B.H. New elevation data triple estimates of global vulnerability to sea-level rise and coastal flooding. Nat. Commun., 2019, 10, 4844.
2. Hauer, M.E.; Hardy, D.; Kulp, S.A. et al. Assessing population exposure to coastal flooding due to sea level rise. Nat. Commun. 2021, 12, 6900. https://doi.org/10.1038/s41467-021-27260-1.
3. Andrew, N.; Bright, P.; Vickers, M.; de la Rua, L.; Teoh, S.J. Coastal proximity of populations in 22 Pacific Island Countries and Territories. PLoS ONE, 2019, 14(9), e0223249. doi:10.1371/journal.pone.0223249.
4. Desmet, K.; Kopp, R.E.; Kulp, S.A.; Nagy, D.K.; Oppenheimer, M.; Rossi-Hansberg, E.; Strauss, B.H. Evaluating the Economic Cost of Coastal Flooding. American Economic Journal: Macroeconomics, 2021, 13 (2): 444-86.
5. Hinkel, J., Lincke, D.; Vafeidis, A.T.; Levermann, A. Coastal flood damage and adaptation costs under 21st century sea-level rise. Proc. Natl. Acad. Sci. U.S.A., 2014, 111, 3292–3297.
6. Kirezci, E.; Young, I.R.; Ranasinghe, R.; Muis, S.; Nicholls, R.J.; Lincke, D.; Hinket, J. Projections of global-scale extreme sea levels and resulting episodic coastal flooding over the 21st Century. Sci. Rep., 2020, 10, 11629. https://doi.org/10.1038/s41598-020-67736-6.
7. Hummel, M.A.; Griffin, R.; Arkema, K.; Guerry, A.D. Economic evaluation of sea-level rise adaptation strongly influenced by hydrodynamic feedbacks. Proc. Natl. Acad. Sci. U.S.A., 2021, 118 (29) e2025961118. https://doi.org/10.1073/pnas.2025961118.
8. Kopp, R.; Horton, R.; Little, C.; Mitrovica, J.; Oppenheimer, M.; Rasmussen, D.J.; Strauss, B.; Tebaldi, C. Probabilistic 21st and 22nd century sea-level projections at a global network of tide gauge sites. Earth's Future, 2014, 2, 383–406. doi:10.1002/2014EF000239.
9. Sweet, W.; Park, J. From the extreme to the mean: Acceleration and tipping points of coastal inundation from sea level rise. Earth's Future, 2014, 2, 579–600. doi:10.1002/2014EF000272.
10. Neumann, J. E.; Emanuel, K.; Ravela, S.; Ludwig, L.; Kirshen, P.; Bosma, K.; Martinich, J. Joint effects of storm surge and sea-level rise on US Coasts: new economic estimates of impacts, adaptation, and benefits of mitigation policy. Clim. Change, 2015, 129, 337–349. doi:10.1007/s10584-014-1304-z.
11. Muis, S.; Verlaan, M.; Winsemius, H.C.; Aerts, J.C.; Ward, P.J. A global reanalysis of storm surges and extreme sea levels. Nat. Commun., 2016, 7, 11969.
12. Li, L.; Switzer, A.D.; Wang, Y.; Chan, C-H.; Qiu, Q.; Weiss, R. A modest 0.5-m rise in sea level will double the tsunami hazard in Macau. Science Advances 2018, 4(8): doi:10.1126/sciadv.aat1180.
13. Nagai, R.; Takabakate, T.; Esteban, M.; Ishii, H.; Shibayama, T. Tsunami Risk Hazard in Tokyo Bay: The Challenge of Future Sea Level Rise. Int. J. Disaster Risk Reduct., 2019, 45, 101321, doi:10.1016/j.ijdrr.2019.101321.
14. Dura, T.; Garner, A.J.; Weiss, R. et al. Changing impacts of Alaska-Aleutian subduction zone tsunamis in California under future sea-level rise. Nat. Commun. 2021, 12, 7119. https://doi.org/10.1038/s41467-021-27445-8.
15. Koyano, K.; Takabatake, T.; Esteban, M.; Shibayama, T. Magnification of Tsunami Risks Due to Sea Level Rise Along the Eastern Coastline of Japan. Journal of Coastal and Hydraulic Structures, 2022, 2, paper no. 12. https://doi.org/10.48438/jchs.2022.0012.
16. Orpin, A.; Rickard, G., Gerring, P.; Lamarche, G. Tsunami hazard potential for the equatorial southwestern Pacific atolls of Tokelau from scenario-based simulations. Nat. Haz. Earth Syst. Sci., 2016, 16, 1239–1257. doi:10.5194/nhess-16-1239-2016.
17. Han, S.-C.; Sauber, J.; Pollitz, F.; Ray, R. Sea Level Rise in the Samoan Islands Escalated by Viscoelastic Relaxation After the 2009 Samoa-Tonga Earthquake, J. Geophys. Res., Solid Earth, 2019, 124(4), 4142—4156. doi:10.1029/2018JB017110.
18. Williams, S.; Titimaea, A.; Bosserelle, C.; Simanu, L.; Prasetya, G. Reassessment of Long-Term Tsunami Hazards in Samoa Based on Sedimentary Signatures. Geosciences, 2020, 10, 481, doi:10.3390/geosciences10120481.
19. Keating, B.H.; Helsley, C.E.; Karogodina, I. 2000.. Sonar Studies of Submarine Mass Wasting and Volcanic Structures off Savaii Island, Samoa. Pure Appl. Geophys. 2000, 157, 1285–1313.
20. Nemeth, K.; Cronin, S. Volcanic structures and oral traditions of volcanism of Western Samoa (SW Pacific) and their implications for hazard education. J. Volc. Geotherm. Res. 2009, 186, 223–237. doi:10.1016/j.jvolgeores.2009.06.010.
21. Roeber, V.; Yamazaki, Y.; Cheung, K.F. Resonance and impact of the 2009 Samoa tsunami around Tutuila. Geophys. Res. Lett., 2010, 37, L21604, doi:10.1029/2010GL044419.
22. Bosserelle, C.; Williams, S.; Cheung, K.F.; Lay, T.; Yamazaki, Y.; Simi, T.; Roeber, V.; Lane, E.; Paulik, R.; Simanu, L. Effects of Source Faulting and Fringing Reefs on the 2009 South Pacific Tsunami Inundation in Southeast Upolu, Samoa. J. Geophys. Res. Ocean. 2020, 125, doi:10.1029/2020jc016537.
23. Bosserelle, C.; Lane, E.; Harang, A. BG-Flood: A GPU adaptive, open-source, general inundation hazard model. Proceedings of the Australasian Coasts & Ports 2021 Conference, 2021, .
24. Yamazaki, Y.; Cheung, K.F.; Lay, T. A self-consistent fault slip model for the 2011 Tōhoku earthquake and tsunami. Journal of Geophysical Research: Solid Earth, 2018, 123(2), 1435-1458.
25. Okada, Y. Surface deformation due to shear and tensile faults in a half space, Bull. Seismol. Soc. Am. 1985, 75(4), 1135-1154.

26. Popinet, S. Quadtree-adaptive tsunami modeling. Ocean Dynamics, 2011, 61(9), 1261-1285, doi:10.1007/s10236-011-0438-z.
27. Vacondio, R.; Palù, A.; Ferrari, A.; Mignosa, P.; Aureli, F.; Dazzi, S. A non-uniform efficient grid type for GPU-parallel Shallow Water Equations models, Environ. Modell. Softw., 2017, 88, 119-137, doi:10.1016/j.envsoft.2016.11.012.
28. Popinet, S. Adaptive modeling of long-distance wave propagation and fine-scale flooding during the Tōhoku tsunami, Nat. Haz. Earth Sys. Sci., 2012, 12(4), 1213-1227, doi:10.5194/nhess-12-1213-2012.
29. Krüger, J.; Kumar, S. Samoa Technical Report: High-resolution Bathymetric Survey. EU-SOPAC Project Report ER 112, Pacific Islands Applied Geoscience Commission, Suva, Fiji, 2008.
30. FUGRO. Report of Survey: Airborne Lidar Bathymetric and Topographic Survey of Samoa 2015. Contract: ECRCR-LIB 2.1, Fugro LADS Document Reference No: TLCS00.047.008, Issue No: 1.00, Fugro LADS Corporation Pty Ltd, South Australia, 2016.
31. Paulik, R.; Horspool, N.; Woods, R.; Griffiths, N.; Beale, T.; Magill, C.; Wild, A.; Popovich, B.; Walbran, G.; Garlick, R. RiskScape: A flexible multi-hazard risk modelling engine. Nat. Haz., 2022, https://doi.org/10.1007/s11069-022-05593-4.
32. Sischka, L.; Bosserelle, C.; Williams, S.; Ting, J.C.; Paulik, R.; Whitworth, M.; Talia, L.; Viskovic, P. Reconstructing the 26 June 1917 Samoa Tsunami Disaster. Appl. Sci. 2022, 12, 3389. https://doi.org/10.3390/app12073389.
33. Tarbotton, C.; Dall'Osso, F.; Dominey-Howes, D.; Goff, J. The use of empirical vulnerability functions to assess the response of buildings to tsunami impact: Comparative review and summary of best practice. Earth-Sci. Rev., 2015, 142, 120–134. https://doi.org/10.1016/j.earscirev.2015.01.002.
34. Reese, S.; Bradley, B.A.; Bind, J.; Smart, G.; Power, W.; Sturman, J. Empirical building fragilities from observed building damage in the 2009 South Pacific tsunami, Earth-Sci. Rev., 2011, 107, 156-173, doi:10.1016/j.earscirev.2011.01.009.
35. IPCC (Intergovernmental Panel on Climate Change). Summary for Policymakers. In: Climate Change 2021: The Physical Science Basis. Contribution of Working Group I to the Sixth Assessment Report of the Intergovernmental Panel on Climate Change [Masson-Delmotte, V., P. Zhai, A. Pirani, S. L. Connors, C. Péan, S. Berger, N. Caud, Y. Chen, L. Goldfarb, M. I. Gomis, M. Huang, K. Leitzell, E. Lonnoy, J.B.R. Matthews, T. K. Maycock, T. Waterfield, O. Yelekçi, R. Yu and B. Zhou (eds.)]. Cambridge University Press. In Press.